

# **Relation of Olfactory EEG to Behavior: Time Series Analysis**

**Behavioral Neuroscience 1986. Vol. 100 No. 5. 753-763**

Walter J. Freeman and Gonzalo Viana Di Prisco  
Department of Physiology-Anatomy University of California, Berkeley

Preparation of this article was supported by Grant MH06686 from the National Institute of Mental Health and by Grant NS16559 from the National Institute of Health.

Gonzalo Viana Di Prisco gratefully acknowledges the support from the Universidad Central de Venezuela.

Correspondence concerning this article should be addressed to Walter J. Freeman, Department of Physiology-Anatomy, University of California, Berkeley, Berkeley, California 94720.

Received for publication May 28, 1985; Revision received October 6, 1985

cc: CREATIVE COMMONS COPYRIGHT: Attribution-Share Alike License

<http://sulcus.berkeley.edu>

Oscillatory electroencephalographic bursts were measured from 64 electrodes implanted on the olfactory bulbs of rabbits. Oscillatory bursts that occurred before and during presentation of odorant conditioned stimuli (CSs) were selected in brief segments. Comparisons between the 64 traces and their spectra showed that, despite amplitude differences between channels, every burst had a common waveform over the entire array. The spectra showed 2 to 5 distinct peaks in each burst. Each trace was fitted with the sum of 5 cosines to express the burst in ten 8 X 8 matrices of amplitude and phase values at its peak frequencies. Two types of burst were identified. Those with dominant frequencies greater than 55 Hz had one narrow dominant spectral peak and reproducible spatial patterns of its amplitude within subgroups of bursts relating to control and odorant CS conditions. Those with dominant frequencies less than 55 Hz were disorderly; their spectra were broad, and their spatial patterns of amplitude did not reproduce within subgroups. A behavioral assay showed that the high- and not the low-frequency bursts contained odor-specific information.

The three aims of this report and the reports of Freeman and Baird (in press) and Freeman and Grajski (1986) are to describe spatiotemporal patterns embedded in the electroencephalograms (EEG) of the olfactory bulb that are specific to odorant conditioned stimuli (CSs), to outline the procedures used to extract and verify these patterns, and to discuss the synaptic mechanisms by which the patterns emerge under classical conditioning. An understanding of these patterns is essential for the design and testing of models representing the nonlinear dynamics of neural ensembles generating the EEG (Freeman 1975, 1979), for localizing and analyzing the cellular mechanisms that underlie associative learning in the olfactory system (Gray, Freeman, & Skinner, 1986), and for undertaking further studies of the integration of the olfactory bulb with the limbic system during behavior (Freeman & Skarda, 1985).

The data base for this study consisted of EEG recordings from arrays of 64 electrodes chronically implanted onto the olfactory bulbs of rabbits. A group of 5

thirsty rabbits was classically conditioned to lick in response to an odorant (CS+) paired with water and not to lick in response to an odorant not paired (CS-; Viana Di Prisco & Freeman, 1985). Recordings were taken during odorant presentations, during immediately preceding control periods, and during rest following satiety. Additional unpublished data (Freeman & Davis, 1984) were taken from 6 rabbits under aversive conditioning by procedures similar to those of Freeman and Schneider (1982).

The main problem encountered was the lack of clear prior specification on what the odor-specific patterns might look like, or where and when they might exist in the bulb. The solution was to fit curves by regression to all of the EEG traces from electrode arrays, so that as much of the variance as possible was incorporated into matrices of coefficients of curves that were optimized with respect to the data in the sense of least squares deviation. Each matrix was tested in turn as a "purified EEG" for its odor-specific information content. (These procedures are described in the present report.) Thereafter, each matrix was further filtered and transformed so as to clarify or further concentrate the information content. These latter procedures are described in detail elsewhere (Freeman & Baird, in press; Freeman & Grajski, 1986; an interpretation of the findings is deferred to the latter report.)

An essential step in the development of this measurement process was to devise a behaviorally related assay of the information content. The assumptions were made that (a) odor-specific neural activity occurred in the bulb during odorant presentation as the basis for the correct CR, (b) the EEG contained odor-specific information arising from the neural activity, (c) the control states before the CS+ and CS- differed from the odor states but not from each other. The data from the appetitively conditioned rabbits served as a test bed. Each animal was kept in a stable response mode to the CS+ and CS- for six sessions. Trials were selected from the last three sessions with a CR+ in response to the CS+ and a CR- in response to the CS-. The CS+ and CS- were presented on randomly interspersed trials (IO of each) in each session. The behavioral assay consisted of a numerical evaluation of the efficacy of purified EEGs to separate and correctly classify the CS+ from the CS- EEGs and these from the control EEGs, without separating the two sets of control EEGs. It was used to reevaluate each step of the process of measurement, which included design of analog and digital temporal filters, the selection of type and number of fitted curves and coefficients, design of spatial filters, optimization of a spatial deconvolution procedure, detection and classification of EEG events as "outliers," determination of which components of the EEG carried odor-specific information and which did not, choice of the number of factors and the types of rotation in factor analysis, evaluation of factorial invariance, and prediction of levels of resolution to be expected with discriminant analysis of the coefficients of the basis functions. In brief, the assay provided corrective feedback for devising procedures to extract behaviorally related information from the EEG, thereby to discern the nature of the neural activity that is manifested in the EEG. A preliminary report and overview has been presented (Freeman & Viana Di Prisco, 1986).

## Method

Rectangular 8 X 8 arrays of 64 electrodes (4 X 4 mm) were prefabricated with their connectors (Eastman, 1975) and were implanted under full surgical anesthesia in accordance with standard aseptic procedures. The arrays were placed directly on the intact dura covering the lateral aspect of the olfactory bulb following removal of the orbital contents and resection of part of the medial wall of the orbit with a drill. An air jet for cooling was used during drilling. The medial, anterior, and ventral bulbar surfaces were not accessible. The orbit was filled with agar made with Tyrode's solution containing 1% Zephiran and was closed with dental cement. Reference and ground leads were placed in the orbit and on the back of the skull.

The recorded signals, monopolar with respect to an orbital electrode, were amplified by fixed-gain (10K) amplifiers with FET inputs. Each channel was analog filtered (-3 dB at 10 Hz and 160 Hz) with a two-stage passive circuit. Frames, consisting of sixty-four 2-hit samples multiplexed at 12  $\mu$ s, were recorded at a 2-ms digitizing interval for 6s. The most significant 8 bits of each sample were stored. Stored traces were displayed on-line with an oscilloscope and examined for artifacts. Six segments (bursts of EEG) 76 ms long (38 points) were selected with pointers under joystick control: three from the control period and three during odorant presentation. Odor segments were chosen from those before and during sniffing (if any) but before licking (if any). Each set of 10 CS+ trials randomly interspersed with 10 CS- trials gave a total of 60 control, 30 CS+ and 30 CS- segments, or bursts. These were stored in blocks with flags indicating whether a lick (CR+), sniff (CR-), or no response (CRO) occurred. Further procedures for amassing and organizing the data base have been described under both appetitive (Viana Di Prisco & Freeman, 1985) and aversive (Freeman & Schneider, 1982) discriminative classical conditioning.

Off-line traces from had channels were replaced by an average of the traces of two adjacent channels (up to 10 in each burst. median near 2). Temporal smoothing consisted of taking the mean of each time point and the two adjacent points. weighted by one-half To remove the residual respiratory wave, a cubic polynomial was fitted to the ensemble average of the 64 traces. This fixed curve was then fitted to each trace with an amplitude parameter and subtracted from the trace to yield the detrended signal. The transfer functions for smoothing and filtering were computed so that their inverse functions could be applied to restore amplitude and phase values derived in subsequent measurements.

Frequency analysis was undertaken using the discrete EVE (Childers, 1978). The 38 points (76 ms) from each channel in each burst segment were padded with zeroes to form 256 points. This allowed finer resolution of the gain and phase spectra generated by the FET. The average gain spectrum for a burst was obtained by calculating the FET gain spectrum for each channel independently, summing these spectra, and dividing by 64. Alternatively, by summing, at each time point over channels and

dividing by 64, the burst ensemble average was obtained. From this time series, the ensemble average gain spectrum was calculated with the FET.

For visual inspection and classification of CS+, CS-, and air-burst spatial patterns, it was necessary to define the respective average patterns. An average pattern, termed centroid, was obtained in two steps. The 38 X 64 points in each burst were reduced to 64 ms values corresponding to the 64 channels. Across the collection of reduced segments in each class, the average rms value of each channel was calculated. This set of 64 values gave the average spatial pattern, or class centroid. Geometrically, the centroid is a point in a 64 dimensional vector space, as is each reduced burst segment. Automated classification of bursts was based on calculation of the distances (Euclidean) between the individual burst vectors and class centroids.

Pairwise correlations of the time series within each burst segment were calculated. The 2,016 unlagged correlation coefficients were transformed by the Fisher  $z$  transform,

$$z = 0.5 \log_e [(1 + r)/(1 - r)], \quad (1)$$

to allow calculation of the distribution mean and standard deviation.

A statistical standard was devised to use as a test bed for procedures of measurement. An 8 X 8 array of 64 sine waves was generated digitally at fixed frequency (60 Hz) and phase (0 radians) but with amplitude that varied with location in the form of a symmetric bivariate normal distribution function with a standard deviation of 1 mm. Spatial patterns of rms amplitude generated from the set replicated the prototypic density plot of the EEG. "Noise" from a Gaussian random number generator with temporal smoothing as for the EEG was added to each trace independently, by channel and burst. This "signal" and "colored noise" were each normalized to 0 mean and unit standard deviation and added at a preset signal to noise ratio (S:N ratio; see below) ranging from 0.01 to 10. Values were truncated to simulate digitizing, smoothed, and detrended by the same procedures used on the EEG.

Measurement of the EEG and of the simulated EEG as time series was based on the selection (to be described) of an appropriate set of basis functions (elementary waveforms or patterns) that defined a coordinate space (Freeman, in press). To express each EEG event as a vector in the coordinate space, a weighted sum of basis functions was fitted by nonlinear regression to a segment of the data. The procedure was most effective when the residuals approached the form of band-limited (colored) noise. The fitted coefficients and nonlinear parameters served as vector components in the coordinate space. When the basis functions and their coefficients were treated separately, the EEG was said to be separated into pure components. The component with the highest signal to noise ratio and the highest fractional energy was termed the dominant component.

Further procedures for analyzing the data base have been described under both appetitive and aversive discrimination (Viana Di Prisco & Freeman, 1985; Freeman & Schneider, 1982). Use of the  $t$  test and the chi-square test to evaluate similarities and differences among EEG patterns has been described by Viana Di Prisco and Freeman (1985) and Freeman & Schneider (1982). The fast Fourier transform (FFT; Childers, 1978) was computed with a program obtained from Programs for Digital Signal Processing (1979). Linear and nonlinear regression with least squares deviation were computed in accordance with procedures described by Golub and Pereyra (1973). The signal to noise ratio (S:N) for the  $k_{th}$  component of the EEG was obtained by summing squares and dividing

$$S:N = \frac{\sum_{i,t} (v_{i,t})^2}{\sum_{i,t} (EEG_{i,t} - v_{i,t})^2}, \quad (2)$$

where  $i = 1, \dots, 64$ ;  $t = 1, \dots, 38$ ;  $v_{i,t}$  were the values of the  $k_{th}$  computed curve. Equivalently the fraction of total energy power integrated over time that was incorporated by the fitted curve was given by

$$E = 100 \frac{\sum_{i,t} (v_{i,t})^2}{\sum_{i,t} (EEG_{i,t})^2}. \quad (3)$$

Computations were done with a Perkin-Elmer Model 3220 in a single-precision 32-bit arithmetic (floating point). All programs for processing and modeling were written in FORTRAN VII and assembled with an optimizing compiler.

## Results

### Preliminary Analysis

The raw EEG consisted of a low-frequency oscillation that was usually but not invariably covariant with respiration, a slow (dc) potential baseline, and high-frequency activity, of which the most obvious feature was the tendency to appear as an oscillatory "burst" during inhalation (see Figure 1). Changes in EEG activity invariably accompanied changes in respiration and or body movement. When these were detected during a control period by automated procedures or by visual editing, the trial was discarded because the behavioral status, with respect to the odor, was indeterminate on that trial.

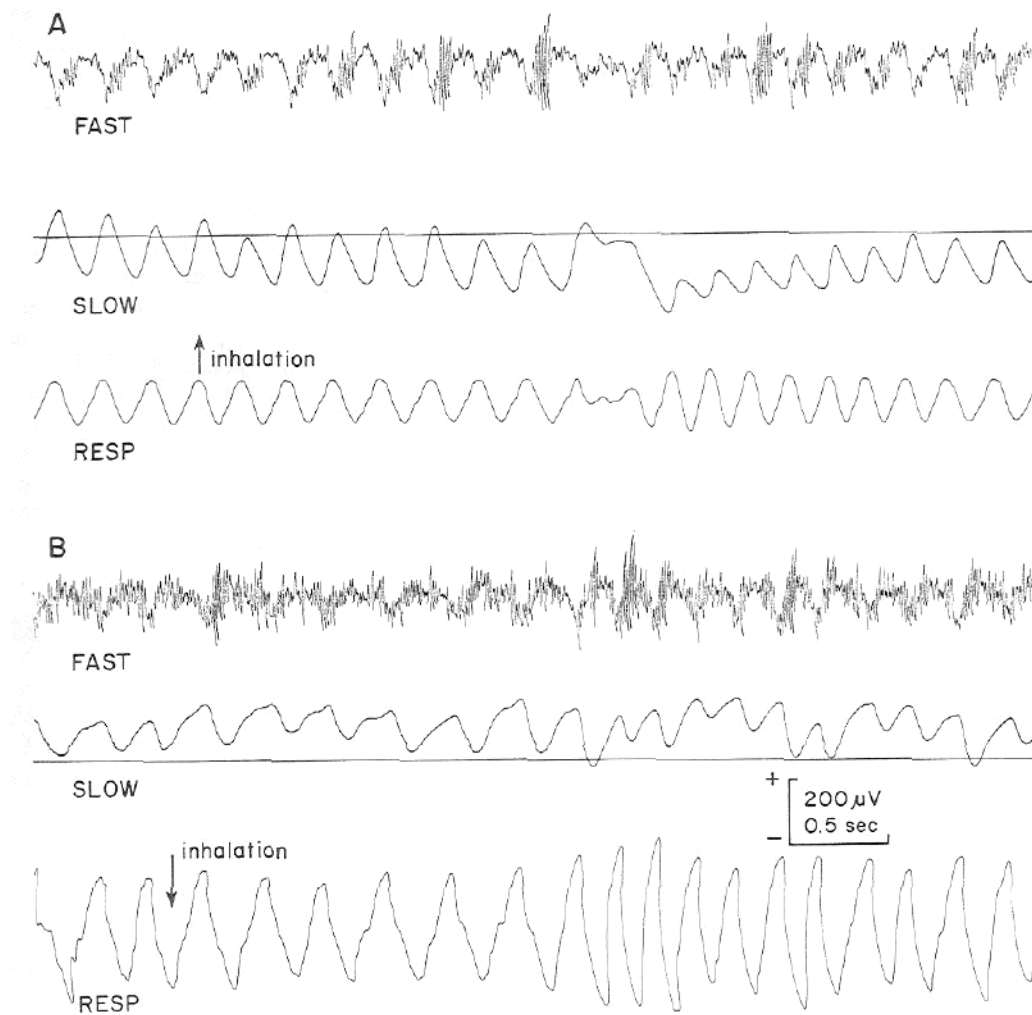


Figure 1. Examples of the EEG from one channel in each of 2 rabbits at rest that were in satiety. (The array electrodes were made from platinized stainless steel. The reference and ground were platinum wires in the orbit adjacent to the may. The upper trace was band-pass filtered [2 stage passive circuit down 3 dB at 10 Hz and 160 Hz]; the middle trace was low-pass filtered [dc to 10 Hz]; the lower trace was from a pneumograph around the chest. A: A spontaneous event [probably swallowing] was manifested by respiratory and EEG changes. B: A spontaneous sniff was manifested by transitory tachypnea accompanied by changes in EEG pattern over the whole array.)

Evaluation of results at this stage was by inspection of contour and density plots of the rms amplitudes of the 64 channels of each burst, and of the spatial ensemble averages (centroids) and standard deviations of sets of rms amplitudes from 10 or more bursts. These spatial patterns revealed a characteristic form for each rabbit, its "signature," as it was easily recognizable but never twice identical (Freeman & Schneider, 1982; Viana Di Prisco & Freeman, 1985).

The internal consistency of bursts was evaluated from the distributions of the 2,016 pairwise correlation coefficients between channels of each burst and accumulated over 20 control bursts as Fisher's  $z$  scores (see Figure 2). These coefficients measured similarity of the normalized waveform across channels and were thus independent of the location of maxima seen in the signature patterns and simulated EEG. These

distributions were comparable with those from the artificial EEG standard at various S:N ratios, saving for a small secondary peak near  $z = 0$  that was traced to occasional deviant channels not detected during editing. These channels were more easily detected by correlating each trace in a burst with the burst ensemble average; traces on channels with  $z < 0.20$  were replaced by the mean of traces on 2 adjacent channels. The median replacement rate was 2.2 channels/burst, but on about 1% of bursts the rate exceeded 10 channels. Those bursts were noted as exceptional and marked for study as outliers.

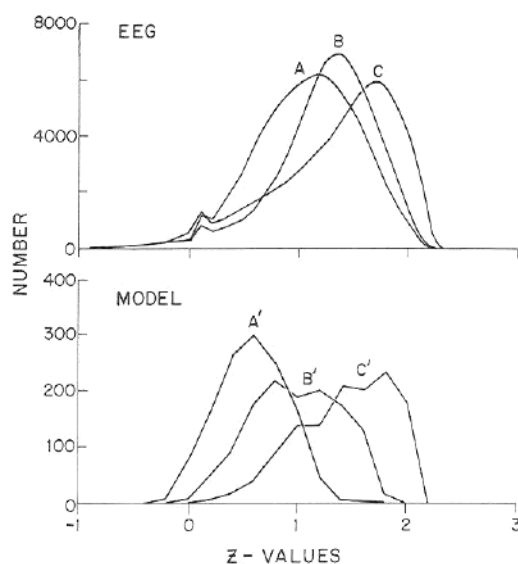


Figure 2. The distribution of pair wise correlation coefficients between channels (2,016/burst). (Upper section: 20 control bursts from 3 rabbits with relatively low [A], moderate [B], and high [C] burst S:N ratios. The values were transformed to Fisher's  $x$  scores. Lower section: The distributions for the artificial EEG standard data with S:N = 0.1 [A], 1.0 [B], and 10 [C]. The small secondary peaks near zero in the upper section were traced to bad channels.)

An empirical relation was found between the S:N ratio of the standard data and the mean  $z$ -value,  $\bar{z}$ :

$$S:N_E = \ln(a + b \bar{z}), \quad (4)$$

where the coefficients  $a = .14$  and  $b = 6.9$  were evaluated by linear regression. This held for the standard with an error  $< 4\%$  over the domain  $.4 > x > 3$  and the range  $.2 > S:N > 5$ . Equation 4 provided an empirical basis for estimating an S:N ratio for each burst as a way of predicting a criterion to which curve fitting should aspire. The distributions of S:N values by this method over sets of bursts were skewed with a grand mean over 5 rabbits of 2.24 and a median of 3.46 (see Figure 5).

Inspection of plots of the 64 traces from representative bursts showed that each had the same number of peaks and zero crossings as the ensemble average time series, although with local variations in peak amplitudes and the times of zero crossings. The correlation analysis suggested that the traces shared a common waveform. Spectral analysis confirmed the inference that the instantaneous temporal frequency was

spatially everywhere the same. Each trace was passed through a Hamming window and padded with zeroes (see the Method section). Figure 3 (upper section) compares the gain spectrum by the FFT of the ensemble average of a representative burst with the average gain spectrum of the 64 channels. Figure 3 (lower section) also shows the close correspondence held also for EEG segments taken between bursts. The essential difference between burst and interburst segments was the lack of a dominant coherent peak in the gain spectrum of the latter.

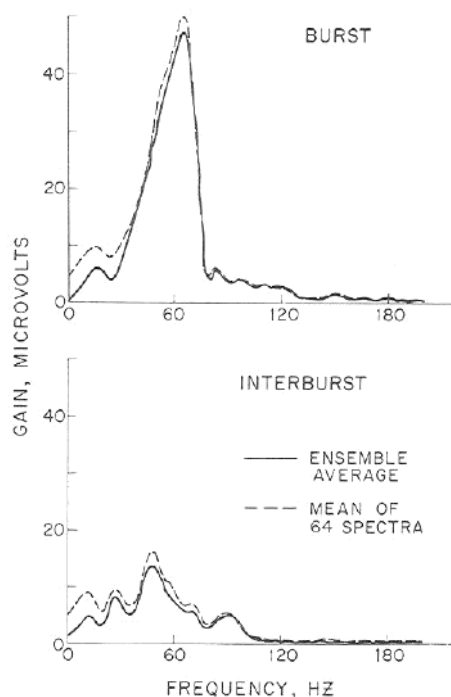


Figure 3. The gain spectrum of the ensemble average compared with the average gain spectrum of the 64 channels for a representative burst from a rabbit at rest and from a representative segment between bursts. (The spectra were computed prior to digital smoothing [passive circuit hand pass filters at 10 Hz and 160 Hz. Spectral peaks at 120 Hz and 180 Hz, when apparent, were traced to harmonics of 60-Hz noise.]

The shapes of the gain spectra from control bursts were consistent. The median peak frequency was between 60 and 70 Hz for 10 of 11 rabbits and between 50 and 60 Hz for 1 rabbit. Values of individual burst peak frequency were occasionally (< 6%) below 40 Hz for all rabbits. The distributions of values greater than 40 Hz were normal for each rabbit, and the values occurred at random without relation to burst amplitude, to sequences of preceding bursts, or to amplitudes or sequences of the respiratory waves accompanying bursts. The coefficient of variation of the channel peak frequencies averaged  $\pm 9.6\%$  from the ensemble average burst frequency (see Table 1). In view of the findings on commonality of waveform, this figure was treated as an estimate of the error of measurement of channel peak frequency.

The FFT generated phase spectra that varied extensively and unpredictably from one burst to the next. An estimate of total within-bursts phase lead or lag was made by adding or subtracting  $2\pi$  radians at each transition from  $\pi$  to  $-\pi$  or vice versa. Averages

over sets of gain and phase spectra from 30 control bursts and interburst segments in each rabbit (see Figure 4) revealed a cumulative phase lead less than  $\pi$  radians; the frequency range of maximal rate of phase increase did not correspond to the location of the peak of the gain spectrum.

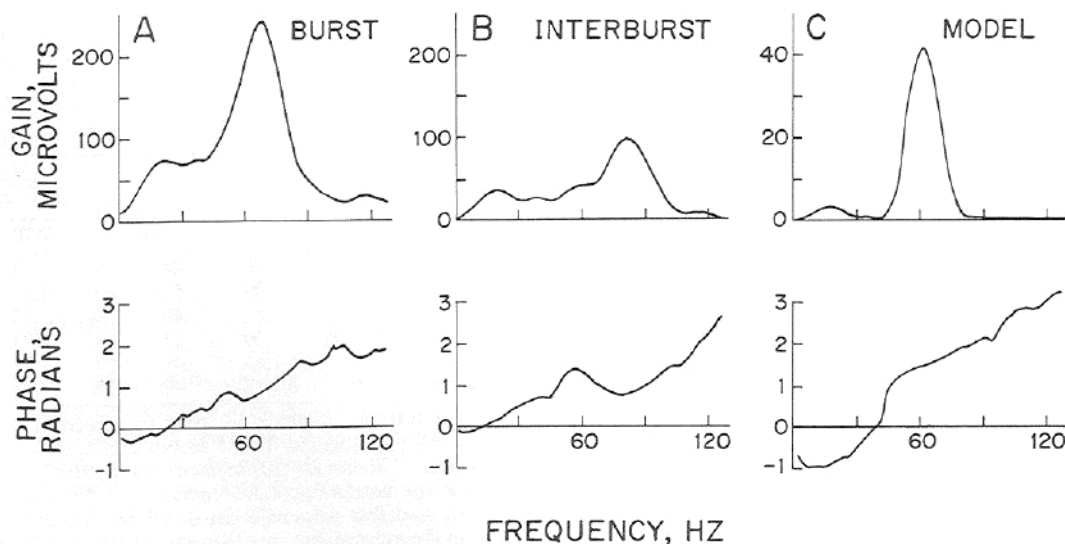


Figure 4, Ensemble averages for the gain and cumulative phase spectra of 30 control bursts, 30 segments between bursts, and 10 simulated bursts with 5:N = 1.0.

These findings were replicated by the FFT of the standard data. The cumulative phase lead (rather than lag) was attributable to the detrending of the data with the cubic polynomial. The width of the spectral peak was determined in the main by the Hamming window applied to these traces of brief duration, but the spectral energy in the EEG was more broadly distributed than that in the simulated data, particularly in the range from 20 to 50 Hz.

Table 1  
*Mean Peak Frequencies (in Hz)  $\pm$  SD*

Subject	Ensemble	Mean channel	C.V.
1	75.38 $\pm$ 6.86	76.11 $\pm$ 14.55	.137 $\pm$ .041
2	75.06 $\pm$ 4.68	76.87 $\pm$ 2.49	.063 $\pm$ .016
3	58.22 $\pm$ 6.50	55.51 $\pm$ 10.54	.094 $\pm$ .023
4	77.82 $\pm$ 12.17	82.38 $\pm$ 13.77	.126 $\pm$ .033
5	74.92 $\pm$ 9.56	77.99 $\pm$ 11.76	.102 $\pm$ .027
6	78.12 $\pm$ 3.71	79.24 $\pm$ 2.12	.051 $\pm$ .016
Average	73.25 $\pm$ 7.24	74.68 $\pm$ 9.21	.096 $\pm$ .028

*Note.* Comparison for 6 rabbits under aversive conditioning between the peak frequency ( $M \pm SD$ ) of the ensemble average (60 bursts for each rabbit) and the average channel peak frequency over 64 channels. The coefficient of variation (C.V.) is the channel frequency SD divided by the mean channel frequency. The average C.V. = 9.6% was interpreted as the error of measurement of channel peak frequency by the FFT.

### Measurement by Curve Fitting

Any basis function with a computable first derivative could be used for measurement. The common tendency to a narrow spectral peak of burst frequency led to the adoption of the cosine as the basis function in this work. Four combinations from a variety of basis functions tested are described to exemplify the procedure:

1. The spectrum of the ensemble average was taken to determine the peak frequency  $f_o$  and the phase at that frequency. These values were used as initial guesses in nonlinear regression to find the amplitude  $v_{oi}$  and phase  $p_i$ ,

$$v_i(t) = v_{oi} \cos(2 \pi f_i t + p_i), \quad (5)$$

$i = 64$ , of each of the traces.

2. The frequency was fixed at the ensemble average peak frequency  $f_o$ , (replacing  $f_i$  by  $\bar{f}_i$  in Equation 5), and the amplitude  $v_{oi}$  and phase  $p_i$ , were found by regression for each channel. These phase values agreed closely ( $r < .95$ ) with the estimates of the phase at the peak frequency  $f$ , from the FFT. The S:N ratios by both methods were unacceptably low (see Figure 5 and Table 2). The curves indicate the S:N ratios derived by various curves fitted to the data. A: A cosine with varying frequency and phase over channels. B: A cosine with fixed ensemble average frequency and varying phase. C: A cosine with varying phase over channels together with amplitude (AM) and frequency (FM) modulation on channels with fixed center burst frequency. D: The sum of a dominant cosine having AM and FM with 4 subsidiary cosines having AM but not FM. E: An empirical estimate of S:N from correlation by Equation 3. Minimal error of measurement was obtained by combining method D with proper editing and spatial filtering. I(C) represents the results of fitting interburst (IB) segments with method C. Overall the tendency is obvious to greater S:N ratios in a state of motivation than in the state of satiety for the same animals, and to higher S:N ratios in bursts (B) than in interburst segments. The same procedures were also applied to interburst segments (see Table 3 and Figure 5); the results showed that IB segments had lower amplitudes and S:N ratios than B segments but that their peak frequencies lay in the same range.

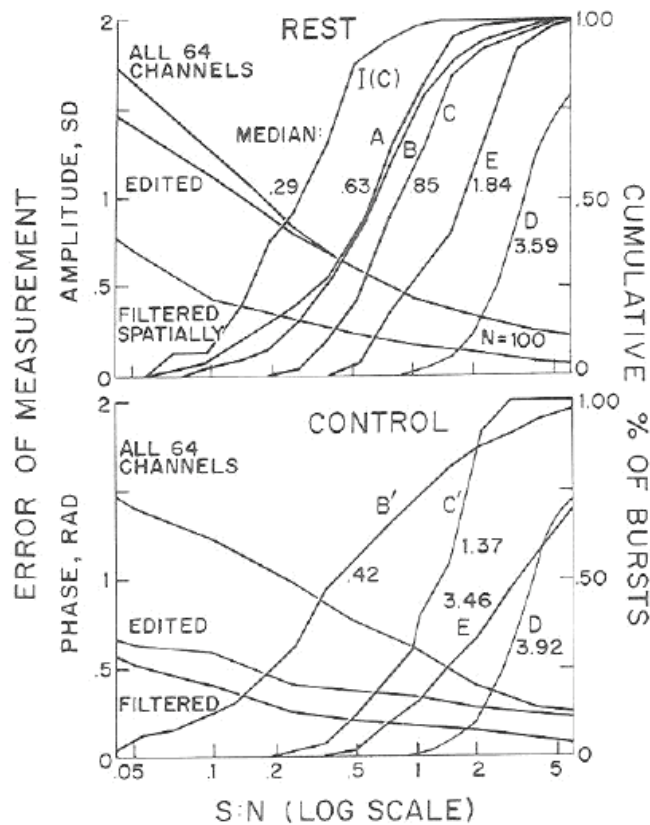


Figure 5. Estimates of signal to noise (S:N) ratios and errors of measurement or phase and amplitude. (The abscissa shows the S:N ratio on a log<sub>10</sub> scale. The ordinates at the left show the standard deviation of amplitude and phase of measurements of simulated standard data from their known 64 values. *Edited* refers to deleting amplitude or phase values for which the correlation coefficient between the trace and the ensemble average was less than 0.2. *Filtered* refers to the use of a spatial low-pass filter as described in Freeman and Baird, in press. The ordinates at the right show percentage of the total number or rest or control bursts [100 bursts total in the upper section comprising 20 from each of 5 rabbits at rest and 300 bursts total in the lower section comprising 60 control bursts from each of 5 rabbits under appetitive conditioning] having at least the S:N ratio on the right ordinate. Rad = radians.)

Table 2  
Normative Measures of S:N Ratio at Rest

Subject	S:N <sub>B</sub>		S:N <sub>C</sub>		S:N <sub>D</sub>		S:N <sub>E</sub>	
1	.37	.20	.43	.19	1.64	.47	2.13	.34
2	1.74	.93	1.99	.99	2.28	.62	1.49	.59
3	2.08	.87	2.24	.80	2.59	.42	1.48	.48
4	.95	.39	1.03	.47	1.72	.39	1.82	.36
5	1.56	1.44	1.56	1.12	2.07	.78	2.29	.31
Average	1.34	.97	1.45	.79	2.06	.56	1.84	.43

Subject	$\bar{z}$	AM: % mean	FM: % mean	SD radians	Aberrant channels
1	1.14	.16	1.5 ± 12.5	-.64	.35
2	.90	.20	.8 ± 11.4	-.51	.20
3	.89	.16	1.1 ± 9.8	-.74	.38
4	1.06	.15	-.5 ± 10.4	.48	.26
5	1.21	.15	1.4 ± 13.7	.76	.30
Average	1.04	.17	.9 ± 11.6	.63	.30

Note. *M* and *SDs* for 5 subjects (20 bursts each) For the signal to noise (S:N) ratios derived by 4 different methods (see text); for amplitude (AM) and frequency (FM) modulation parameters expressed as percentage of center amplitude and frequency: for the SD of phase *p* over the 64 channels for the mean of pairwise correlation coefficients expressed as Fisher's *z* scores: and the

average number of channels/burst on which a trace was replaced by its neighbors owing to a low correlation with the ensemble average ( $r < .2$ ).

Table 3  
Comparison of 20 Bursts and 20 Interburst Segments

Subject	rms + SD				Peak frequency ± SD			
	B		IB		B		IB	
1	12.3	3.2	9.5	2.1	77.5	7.3	77.4	13.4
2	7.5	1.2	5.1	1.1	64.3	3.6	68.4	10.6
3	12.7	1.9	6.9	1.1	63.3	3.3	66.1	10.9
4	6.5	1.0	3.3	0.9	78.6	5.9	69.4	13.7
5	11.3	1.5	4.8	1.1	79.6	5.9	73.9	11.9
Average	10.1	1.9	5.9	1.3	72.6	5.4	71.1	12.2

Subject	S:N <sub>B</sub> ± SD				log <sub>10</sub> chi-square	
	B		IB		B×B	B×IB
1	.37	.20	.24	.14	.21	2.24
2	1.74	.93	.53	.45	1.61	3.61
3	2.08	.87	.46	.30	.53	2.70
4	.95	.39	.26	.14	.95	3.35
5	1.56	1.44	.49	.27	.97	3.66
Average	1.34	.88	.40	.28	.85	3.11

*Note.* The rms amplitudes ± SD, peak frequencies ± SD, and signal to noise ratios h method B for 5 rabbits at rest, in order to compare burst (B) and interburst (IB) segments of the EEG. Use of the chi-square test (Viana Di Prisco & Freeman, 1985; Freeman & Schneider, 1982) showed that pairs of B did not differ significantly from each other on the average, but that IB segments had significantly different (> 2.00) spatial patterns from bursts, even though the ensemble spatial averages of rms values of B and IB segments yielded the same signature pattern characteristic of each rabbit.

3. The amplitude and frequency of the cosine were varied linearly with time about the center amplitude  $v_{oi}$ , and frequency  $f_o$  over the burst duration,

$$v_i(t) = v_{oi} [1 + AM_i(t - t_m)] \cdot \cos [2\pi t (f + FM_i(t - t_m)) + p_i], \quad (6)$$

where  $t_m$  was the center time,  $AM_i$  was an amplitude modulation coefficient, and  $FM_i$  was a frequency modulation coefficient for each channel. Figure 6 shows three examples of relatively complicated bursts fitted with Equation 6. For most bursts there was substantial residual (see Table 2).

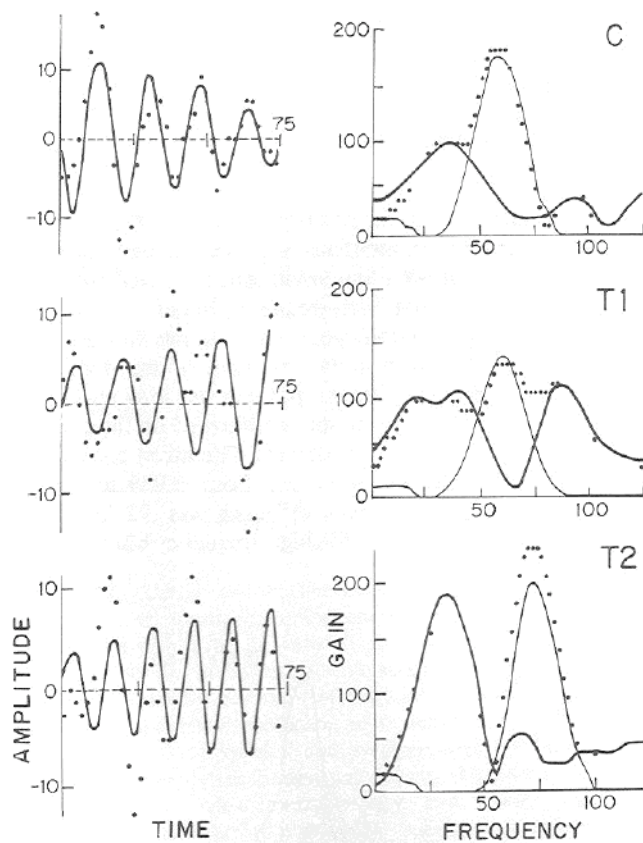


Figure 6. Three examples of the ensemble averages of control bursts (dots in left section) and their spectra by the FFT (right section). (The thin curves from Equation 6 represent the fitted curves and their spectra: the thick curves show the residuals and their spectra. The residuals were fitted with the sum of four cosines; the residuals in the ensemble averages were less than 3% of the total energy in the ensemble average. The same appearance of multiple low peaks in the spectra of the residuals was seen in the spectra of simulated standard data at low signal to noise ratios. C = control burst; T1 = 1st test burst; T2 - 2nd test burst.)

4. A curve was fitted to the residual. This consisted of the sum of four cosines. After Equation 6 was fitted to the ensemble average in the time domain, the curve was subtracted and the FFT was taken of the residual. The peak frequency and phase were identified, and Equation 6 was fitted to the residual and subtracted. This was repeated to give a total of five cosines at five frequencies. The sum was fitted by regression to the 64 traces to give the amplitude patterns of the five components and the phase of the dominant component. In this approach the estimated S:N ratios approached those predicted by the empirical method (Figure 5, section E and Equation 4). The distributions of burst energy among the 5 components and the residuals are shown in Figure 7, which were pooled for control and odor bursts from 5 rabbits. The standard data also provided a basis for estimating the precisions of measurement of amplitude and phase at the peak frequency. These were expressed as the standard deviation of the phase from zero mean and the standard deviation of the amplitude from the distribution of the peak amplitudes of a standard data set with zero noise. As shown in Figure 5, the errors of measurement increased exponentially with decreasing S:N ratio, but with substantial improvement in precision of measurement, of phase if outlier channels were deleted and in amplitude if spatial filtering was used, as described in a report by Freeman and Baird in press. Given an estimate of the S:N ratio following

measurement of a burst, this graph was used to estimate the confidence intervals of the resulting amplitude and phase values.

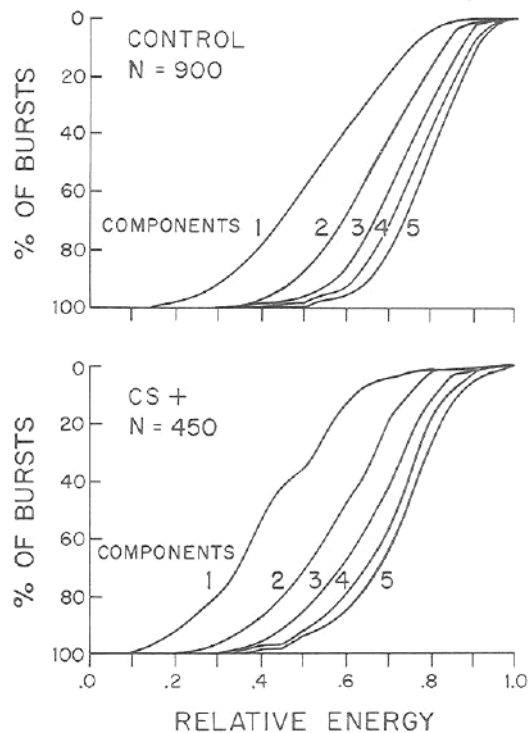


Figure 7. Curves showing the percentage of total bursts having at least the designated fraction of energy in the designated component. (For example, among control bursts, at least 50% of bursts had about 50% of their energy in the dominant component.)

### Analysis of the Components

Inspection of density plots of the spatial amplitude patterns of the five components showed no significant departures from the "signature" patterns of the rabbits (see Figure 8). The matrix of correlation coefficients among the five components, averaged by  $z$  transform across bursts and subjects, gave values for  $\bar{r}$  ranging from .69 to .97 with a grand mean of .83; there was no dependence on subject or on the component pairs. This result further substantiated the findings on commonality of waveform across the array.

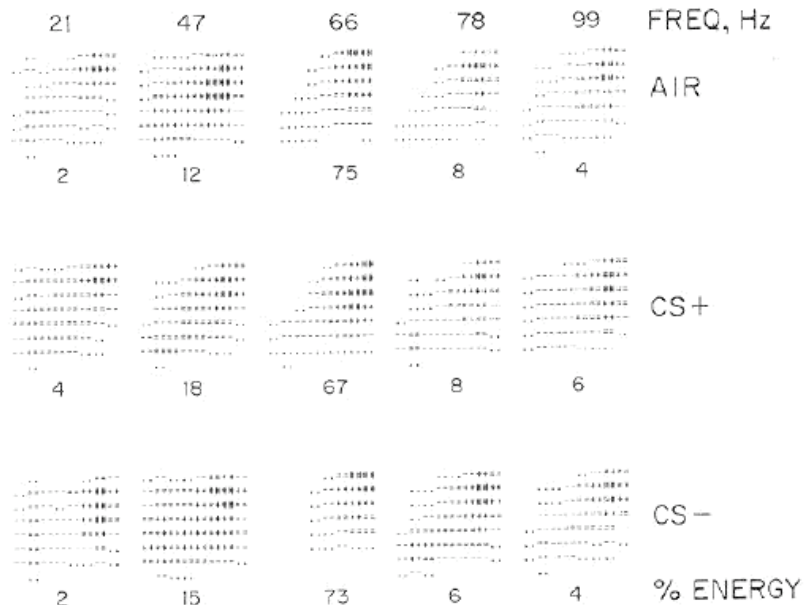


Figure 8. Density plots from a conditioned rabbit of the ensemble averages (centroids) of the amplitude patterns of the 5 components across 20 control bursts, 10 CS+ (conditioned stimulus) bursts, and 10 CS- bursts. (The frequencies at the top are the mean values for the entire sets of 5 components. The fraction beneath each density plot is the mean fraction of the total energy taken by those components. The 7-level scale [in decreasing order] is [# \* + = - . ] with blank corresponding to the lowest amplitude in each frame. The left edge of each frame is at or near the posterior border of the bulb; the right edge is near the center of the lateral wall of the bulb; the top edge is dorsal.)

The range of values for the five frequencies from 8 to 122 Hz reflected the pass band of the temporal filters. The median interval between frequencies within bursts was 19.3 Hz but the standard deviation of the distribution ( $\pm 9.3$  Hz) was nearly half of the mean (22.1 Hz). There was no evidence for regularities to suggest harmonics within and across bursts.

Bursts seldom shared a large energy content at both high and low frequencies. Figure 9 shows a histogram of the difference (ED) between the energy fraction of the largest component with frequency  $f_1 > 60$  Hz less the energy fraction of the largest component  $f_1 < 60$  Hz. On the average, only 10% of control bursts were dominantly low frequency, but 41% of odor bursts showed this trait. The preponderance of low-frequency bursts (typically at lower amplitude) accounted largely for the mean reduction in burst amplitude with odor presentation (Viana Di Prisco & Freeman, 1985) and entirely for a mean reduction in burst frequency.

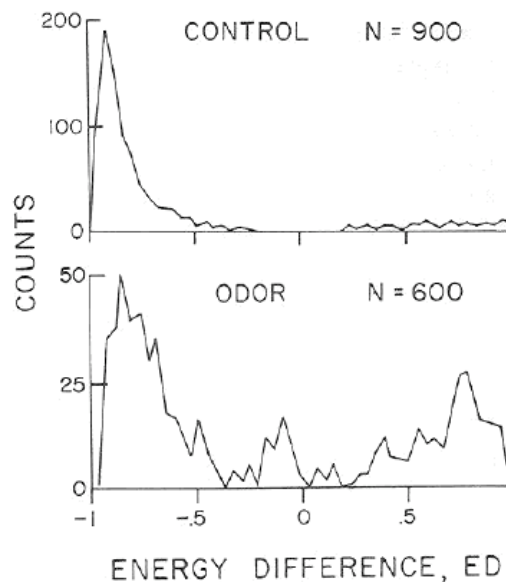


Figure 9, Distributions by histogram for 900 control bursts and 600 odor (pooled from 5 rabbits) of the difference (ED) between the fraction of energy within the burst of the largest component with a frequency 60 Hz less the fraction of the largest component with a frequency of < 60 Hz. (In both groups the energy tended to be concentrated to one side or the other of the spectrum and was seldom balanced (differences near zero). By this criterion the low-frequency bursts were 3 to 4 times more likely to occur during odor presentation and sniffing than during the control period.)

The bursts with low dominant frequency differed from the high dominant frequency in several respects in addition to their preponderance in odor periods. Figure 10 shows their spectral properties by a histogram of the five frequencies, each weighted by its relative fraction of energy after correction for the effects of the temporal filters which compared bursts with dominant frequencies greater and less than 60 Hz. On the average the spectral spread of the low-frequency bursts was greater. Two other measures confirmed this. Figure 11 (upper section) shows the mean fraction of energy in the dominant component over spectral domains 10 Hz in width ranging upward from 10 Hz. The highest concentration of energy into the dominant component occurred for dominant frequencies of 60-70 Hz. The mean and standard deviation of the FM coefficient were similarly evaluated over subranges of the dominant frequency (Figure 11, lower section); the mean value expressed as percentage of center frequency was positive (frequency acceleration) for bursts above 60 Hz; the standard deviation increased exponentially with decreasing frequency. These features all showed that low-frequency bursts were less coherent temporally than high-frequency bursts.

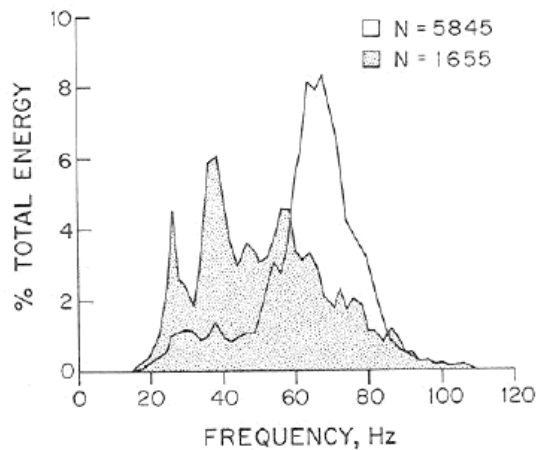


Figure 10. Average spectra of low- and high-frequency bursts, showing that the dispersion of spectral energy was greater in the former than in the latter.

Evaluation of spatial coherence across bursts was done by within-groups correlation of the matrices of the dominant component amplitudes. Density plots of the low- and high frequency bursts showed that both conformed on the average to the "signature" patterns of subjects. The mean correlation coefficient by  $z$  transform (bounded from  $-.999$  to  $+.999$ ) within the high-frequency control bursts was  $.92$  (averaged over subjects); those between the high-frequency bursts within the CS+ and CS- groups were, respectively,  $.83$  and  $.86$ ; but the average between the low-frequency bursts was  $.12$ , ranging from  $.04$  to  $.26$  over subject, control, and CS+ or CS- subgroups. In brief, the low-frequency bursts were spatially as well as temporally disorderly, when viewed as samples taken repeatedly from the larger population of bursts.

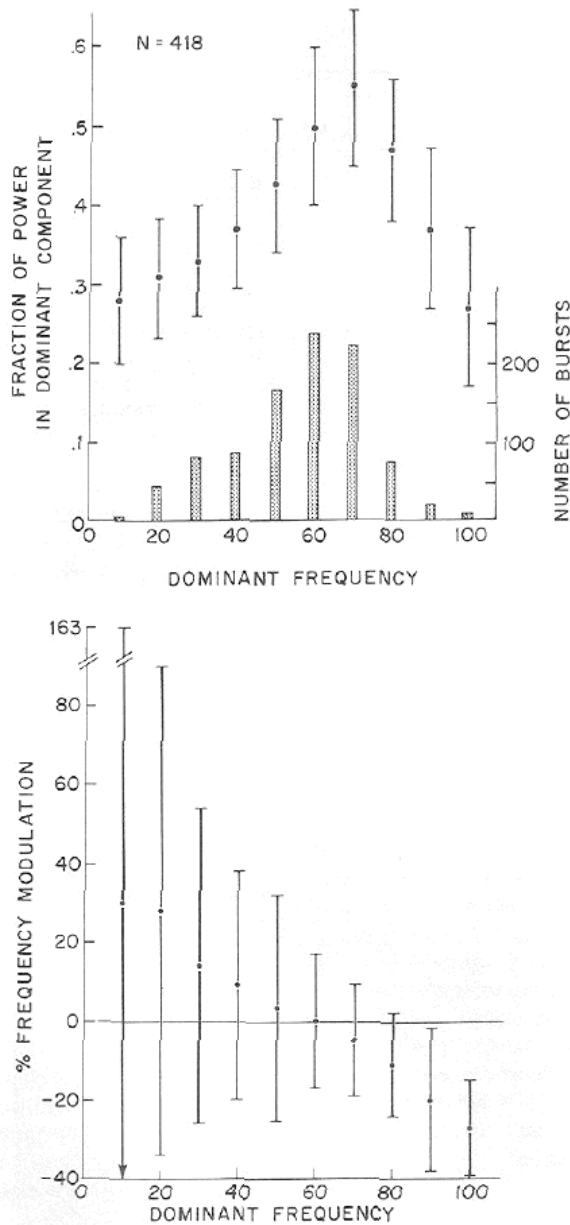


Figure 11, Upper section: The mean and SD of the fraction of energy in the dominant component computed for bursts having frequencies within the indicated frequency bands. (The bar graph shows the number of entries into each subgroup.) Lower section: The mean and standard deviation of frequency modulation (FM), the frequency modulation coefficient in Equation 5 expressed as percentage of center frequency and averaged over the bursts having dominant frequencies in the designated bands. (High-frequency bursts on the average tended toward negative FM (slowing), and low-frequency bursts tended to positive FM (quickening) but with much higher standard deviations of FM. Both graphs indicated greater temporal incoherence in low-frequency bursts. The amplitude modulation (AM) parameter depended on whether the burst was taken during the onset (positive AM), middle, or end (negative AM) of the burst: there was a small negative correlation ( $\bar{r} = .227$ ,  $n = 1156$ ,  $p < .01$ ) between AM and FM in the high-frequency bursts as predicted on theoretical grounds (Freeman, 1975), but it sufficed to account for less than 5% of the variance in FM on the basis of centering during the editing of the bursts with the joystick control.)

## The Search for Odor-Specific Information

The preponderance of low-frequency bursts in odor trials raised the question, which of these two types, if either, contained odor-specific information? The answer was provided by use of a burst classification procedure. The bursts from each subject were grouped into four sets: control C+, control C-, odor CS+, and odor CS-. The centroid was calculated for the 64 dominant component amplitudes of each set. Then the Euclidean distance was calculated for each control burst between its own centroid and the apposing control centroid; if the distance to its own centroid was less than the distance to that apposing, the burst was tagged as correct. The result was expressed as percentage correct over the combined C+ and C- sets (see Figure 12, upper section). The procedure was repeated for the odor bursts and centroids (lower section). The behavioral assay was the percentage of correct odor bursts minus the percentage of correct control bursts, on the premise that the two sets of control bursts were not from significantly different populations. The requirement was imposed that the percentage of correct control bursts not exceed 60%.

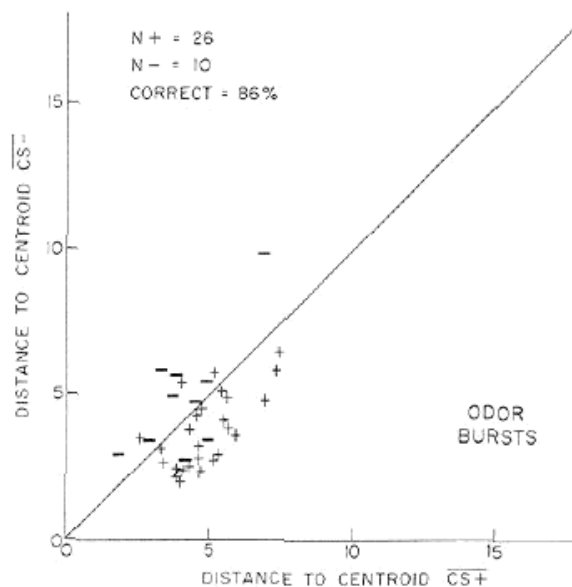
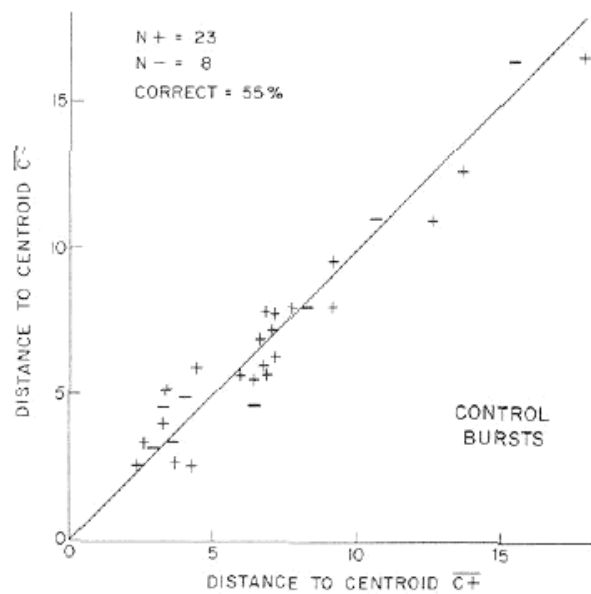


Figure 12. Example of the use of a Euclidean distance measure of burst similarity to test for the separation and correct classification of the CS+ and CS- odor bursts without significant separation of the two sets of control bursts, C+ and C-. (These data were further processed by methods described in Freeman and Baird [in press]. CS = conditioned stimulus; C = control state.)

Optimal results were obtained from the 4 of 5 rabbits that showed behavioral evidence for discrimination between the CS+ and CS- and from only those trials on which a correct CR+ or CR- occurred. The EEG bursts from 1 rabbit that showed no behavioral evidence for discrimination could not be classified in respect to CS. The behavioral assay was calculated repeatedly, first while deleting bursts with dominant frequencies less than a cut-off frequency shifted upwardly from 30 Hz to 70 Hz in steps of 5 Hz, and then while deleting bursts with frequencies greater than the cut-off frequency shifted downwardly from 90 Hz to 50 Hz in steps of 5 Hz. Unequivocally, the results (see Figure 13) showed that the CS+ and CS- odor bursts could be correctly classified to a significant degree in respect to the odors on the basis of the amplitudes of the dominant components of the high-frequency bursts but not those of the low-frequency bursts.

The percentage difference assay was increased by deletion as well of bursts with absolute frequency modulation (FM) > 50% and bursts with <.15 fraction of energy in the dominant component, that is, the bursts with other direct signs of low temporal coherence. The distributions of orderly and disorderly bursts by these three criteria are shown in Table 4 for the 5 subjects. They were grouped in respect to whether a CS was present and whether a correct CR occurred. The preponderance was 2.5:1 of disorderly bursts in the test periods as compared with control periods, but the incidence was not significantly different in respect to trials in which a correct CR did or did not appear.

Table 4  
Occurrence of Orderly Versus Disorderly Bursts

Subject	Stimulus: control		Stimulus: test		Response: correct		Response: incorrect	
	Orderly	Disorderly	Orderly	Disorderly	Orderly	Disorderly	Orderly	Disorderly
1	136	44	72	108	104	70	104	82
2	149	31	97	83	137	61	109	53
3	169	11	122	58	165	48	126	21
4	122	58	80	100	144	114	58	44
5	159	21	123	57	52	14	230	64
%	81.7	18.3	54.9	45.1	66.2	33.8	70.4	29.6

*Note.* Numbers of bursts classified as disorderly versus orderly by three criteria with respect to their temporal properties: frequency of the dominant component in the ensemble average  $\bar{f}_1 < 55$  Hz; absolute value of the frequency modulation parameter expressed as percentage (%) of center frequency FM > 50%; or fraction of total burst energy incorporated into the dominant component less than 0.15. By these criteria the disorderly bursts were 2.5 times more likely to occur in test periods than in control periods, but the incidence was not significantly different between trials with or without a correct CR.

The assay was also applied to the amplitudes of the secondary and tertiary components; no significant separation of CS+ and CS- resulted. Inclusion of the secondary component of low-frequency bursts when it exceeded 55 Hz resulted in

diminished separation of bursts. This was predicted on the basis of commonality of waveform.

The data in Figures 12 and 13 are for illustrative purposes; they were processed further by methods described in reports by Freeman & Baird (in press) and Freeman & Grajski (1986), in which the statistical significance and confidence intervals of the percentage difference assay are discussed. Here it may suffice to state the conclusion that the odor-specific information was found only in the amplitude matrices of the dominant component of the high-frequency bursts, and only in those rabbits showing clear behavioral evidence of odor discrimination.

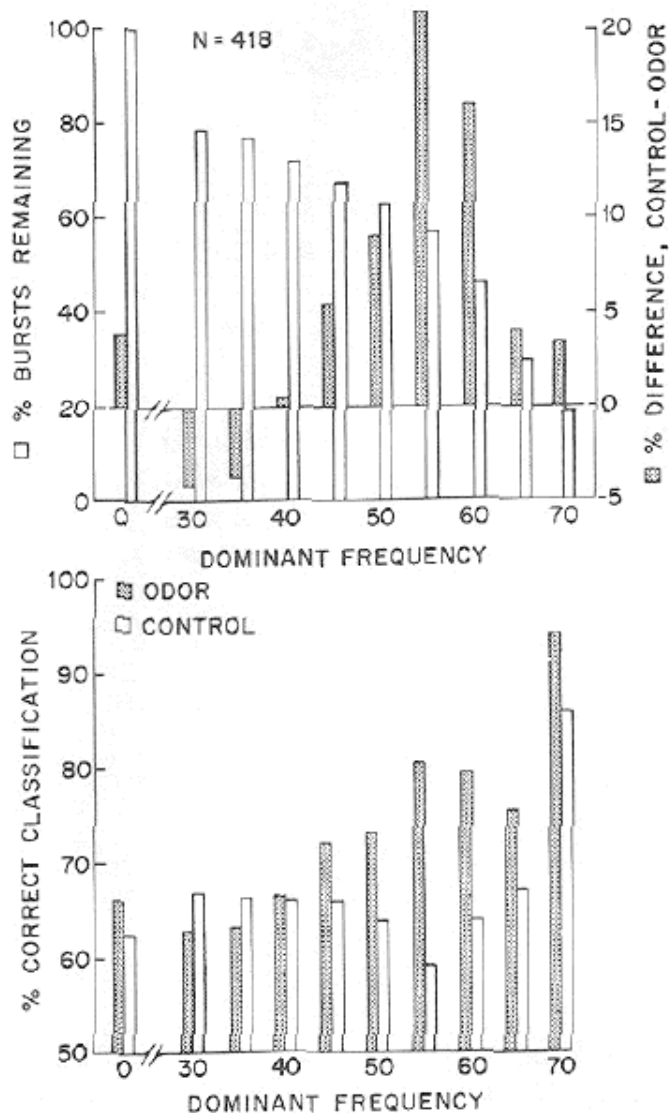


Figure 13. Lower section: The pooled results from 4 rabbits of the % correct classification of control (open bars) and odor (stippled) bursts as a function of the deletion of bursts having dominant component Frequencies less than the indicated values. Upper section: The difference (stippled bars) between the percentage correct odor bursts less the percentage correct control bursts. (The open bars shows the fraction of bursts remaining after the deletion. Again, these data were further processed by methods to be described [Freeman & Baird, in press]: the main point here is that odor-specific information was detected in the high- and not the low-frequency bursts, even though the latter

occurred more commonly in odor periods than during control periods. The statistical power of the assay is evaluated in Freeman and Grajski [1986].)

## **Discussion**

Three findings in this study are most noteworthy. First, despite marked amplitude differences between channels that underlay the signature pattern of each subject and the random departures from it, the same time series held for almost all channels on almost every burst. Visual inspection of randomly selected departures from this rule showed that they were almost all attributable to transient electrode noise, or to unusually low-burst amplitude on channels far from the center focus of activity near an edge of the array. This finding of commonality was supported by examination of representative time series, by the distributions of pairwise channel correlation coefficients, by the near congruence of spectra of the ensemble average with average spectra over the ensemble, and by the high correlations of the spatial patterns of the amplitudes of the five components following burst decomposition. The near congruence of the temporal spectra of interburst segments and of their class centroids with those of bursts indicated that the interburst activity had this property also.

Second, bursts fell into two classes. Those with dominant frequencies of 55 Hz or greater were more orderly, in the sense that they had a larger fraction of the total energy in one spectral band, there was less frequency modulation, and the spatial patterns of the amplitude of the dominant component were more reproducible across classes of bursts. Those with frequencies less than 55 Hz had lower amplitude, less concentration of energy in the dominant component, greater frequency modulation, and no tendency to form reproducible spatial patterns across sets of control or odor bursts, other than conformance on the average to the signature pattern. Interburst segments shared these properties of disorderly bursts, but with one major difference. The peak frequency of the interburst segments was seldom below 55 Hz, and the mean peak frequency was near the mean peak frequency of orderly bursts in each subject.

Third, information that served to classify bursts correctly with respect to control, CS+ and CS- odor conditions was found in the orderly bursts and not in the disorderly bursts.

The method of EEG decomposition with AM-FM cosines was adopted because empirically it appeared to be best suited to the form of the data. No claim is made that this is the only way or even the best way to decompose the EEG, but this method does make it easier to correct components for the effects of prior temporal filtering and to undertake spatial filtering.

Further interpretation is deferred until the results of spatial analysis have been described. The main import of the present findings is statistical. Prior attempts to find odor-specific information in the spatial patterns of burst amplitude and phase under conditions of odor discrimination have failed (Freeman & Schneider, 1982; Viana Di

Prisco & Freeman, 1985). One reason now apparent for this failure is the inclusion in the analysis of all bursts irrespective of type. The disorderly bursts appear not to conform to any predictable subclass in respect to spatial amplitude; instead they contribute a large variance to the groups of orderly bursts, especially those in CS+ and CS- groups in which the disorderly bursts are most likely to occur. This suggests that they should be treated as outliers. However, deletion of them must be justified by a physiological explanation of how they are generated by the bulb and what they signify for behavior. These aspects are considered further in reports elsewhere (Freeman & Baird, in press; Freeman & Grajski, 1986), and in theoretical and methodological reviews (Freeman & Viana Di Prisco, 1986; Freeman, 1986).

## References

Childers, D. G. (1978). *Modern spectrum analysis*. New York: IEEE Press. Digital Signal Processing Committee. (Ed.). (1979). *Programs for Digital Signal Processing*. New York: IEEE Press.

Eastman, C. (1975). Construction of miniature electrode arrays for recording cortical surface potentials. *Journal of Electrophysiological Techniques*, 5, 28-30.

Freeman, W. J. (1975). *Mass action in the nervous system*. New York: Academic Press.

Freeman, W. J. (1979), EEG analysis gives model of neuronal template-matching mechanism for sensory search with olfactory bulb. *Biological Cybernetics*, 35, 221-234.

Freeman, W. J. (in press), Analytic techniques used in the search for the physiological basis of the EEG. In A. Gevins & A. Remond (Eds.), *handbook of electroencephalography and clinical neurophysiology* (Vol. 3A, Part 2, chap. 14). Amsterdam, The Netherlands: Elsevier.

Freeman, W. J., & Baird, B. (in press). Relation of olfactory EEG to behavior: Spatial analysis. *behavioral Neuroscience*.

Freeman, W. J., & Davis, G. W. (1984). [Aversive conditioning of rabbits to olfactory stimuli: EEG recordings.] Unpublished raw data.

Freeman, W. J., & Grajski, K. A. (1986). Relation of olfactory EEG to behavior: Factor analysis. Manuscript submitted for publication.

Freeman, W. J., & Schneider, W. S. (1982). Changes in spatial patterns of rabbit olfactory EEG with conditioning to odors. *Psychophysiology* 19, 44-56.

Freeman, W. J., & Skarda, C. S. (1985), Spatial EEG analysis, nonlinear dynamics, and perception: The neo-Sherringtonian view. *Brain Research Reviews*, 10, 147-175.

Freeman, W. J., & Viana Di Prisco, G. (in press). EEG spatial pattern differences with discriminated odors manifest chaotic and limit cycle attractors in olfactory bulb of rabbits. *Proceedings of the First Trieste Meeting on Brain Theory* (pp. 97-120). Berlin: Springer-Verlag.

Golub, G. H., & Pereyra, V. (1973). The differentiation of pseudo-inverses and nonlinear least squares problems whose variables separate. *Society for Industrial and Applied Mathematics, Journal on Numerical Analysis*, 10, 413-432.

Gray, C. M., Freeman, W. J., & Skinner, J. W. (1986). Chemical dependencies of learning in the rabbit olfactory bulb: Acquisition of the transient spatial-pattern change depends on norepinephrine. *Behavioral Neuroscience*, 100, 585-596.

Viana Di Prisco, G., & Freeman, W. J. (1985). Odor-related bulbar EEG spatial pattern analysis during appetitive conditioning in rabbits. *Behavioral Neuroscience*, 99, 964-978.

---

*(END DOCUMENT)*